Article

Neuron

Regulation of Recurrent Inhibition by Asynchronous Glutamate Release in Neocortex

Graphical Abstract

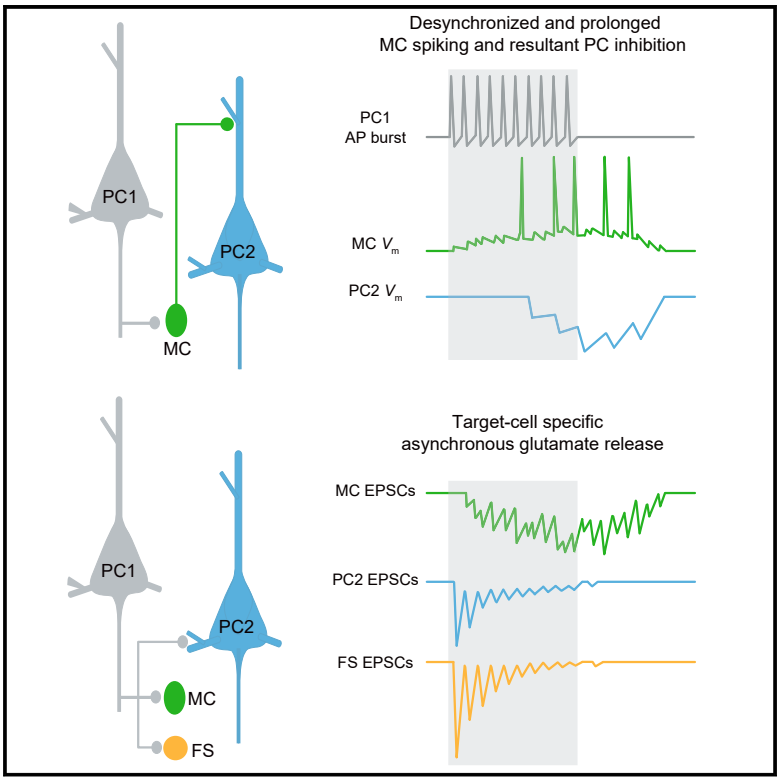

Highlights

- PC burst induces desynchronized and prolonged MC firing and slow recurrent inhibition
- Glutamate AR occurs at PC-MC synapses, causing desynchronized and prolonged MC firing
- The AR strength is target-cell specific and presynaptic PC-subtype dependent
- Syt7 and background Ca^{2+} regulate AR strength and thus slow recurrent inhibition

Authors

Suixin Deng, Junlong Li, Quansheng He, ..., Qiang Dong, Ying Mao, Yousheng Shu

Correspondence

yousheng@fudan.edu.cn

In Brief

The timing and size of inhibition are crucial for cortical processing. Deng et al. report that long-lasting asynchronous glutamate release from excitatory synapses regulates the operation of a recurrent-inhibition microcircuit mediated by Martinotti cells through prolonging and desynchronizing their firing.

Deng et al., 2020, Neuron *105*, 1–12
February 5, 2020
https://doi.org/10.1016/j.neuron.2019.10.038

CellPress

Please cite this article in press as: Deng et al., Regulation of Recurrent Inhibition by Asynchronous Glutamate Release in Neocortex, Neuron (2019), https://doi.org/10.1016/j.neuron.2019.10.038

Neuron
Article

Regulation of Recurrent Inhibition by Asynchronous Glutamate Release in Neocortex

Suixin Deng,[1] Junlong Li,[1] Quansheng He,[1] Xiaoxue Zhang,[2] Jie Zhu,[3] Liang Li,[1] Zhen Mi,[1] Xiufeng Yang,[3] Man Jiang,[4] Qiang Dong,[2] Ying Mao,[2] and Yousheng Shu[1,2,5,*]

[1]State Key Laboratory of Cognitive Neuroscience and Learning & IDG/McGovern Institute for Brain Research, Beijing Normal University, 19 Xinjiekou Wai Street, Beijing 100875, China

[2]Department of Neurology, Huashan Hospital, State Key Laboratory of Medical Neurobiology, Institutes for Translational Brain Research, MOE Frontiers Center for Brain Science, Fudan University, Shanghai 200032, China

[3]Institute of Neuroscience and State Key Laboratory of Neuroscience, Chinese Academy of Sciences, 320 Yueyang Road, Shanghai 200031, China

[4]Department of Physiology, School of Basic Medicine and Tongji Medical College, Huazhong University of Science and Technology, Wuhan 430030, China

[5]Lead Contact

*Correspondence: yousheng@fudan.edu.cn

https://doi.org/10.1016/j.neuron.2019.10.038

SUMMARY

The timing and size of inhibition are crucial for dynamic excitation-inhibition balance and information processing in the neocortex. The underlying mechanism for temporal control of inhibition remains unclear. We performed dual whole-cell recordings from pyramidal cells (PCs) and nearby inhibitory interneurons in layer 5 of rodent neocortical slices. We found asynchronous release (AR) of glutamate occurs at PC output synapses onto Martinotti cells (MCs), causing desynchronized and prolonged firing in MCs and thus imprecise and long-lasting inhibition in neighboring PCs. AR is much stronger at PC-MC synapses as compared with those onto fast-spiking cells and other PCs, and it is also dependent on PC subtypes, with crossed-corticostriatal PCs producing the strongest AR. Moreover, knocking out synaptotagmin-7 substantially reduces AR strength and recurrent inhibition. Our results highlight the effect of glutamate AR on the operation of microcircuits mediating slow recurrent inhibition, an important mechanism for controlling the timing and size of cortical inhibition.

INTRODUCTION

The timing and amount of recurrent synaptic inhibition are critical for the dynamic balance of excitation and inhibition and the regulation of information processing in cortical networks. GABAergic interneurons that mediate synaptic inhibition show great diversity in their morphology, firing patterns, synaptic plasticity, and gene expression (Markram et al., 2004; Moore et al., 2010); different interneuron types display unique functions in the network (Blackman et al., 2013; Jonas et al., 2004; Pouille and Scanziani, 2004; Silberberg, 2008; Stefanelli et al., 2016; Wilson et al., 2012). Previous studies revealed the cellular composition, synaptic connectivity, and dynamics of inhibitory microcircuits in both hippocampus (Mittmann et al., 2004; Pouille and Scanziani, 2004) and neocortex (Silberberg, 2008). Parvalbumin (PV)-positive fast-spiking (FS) basket cells are the potential interneuron type mediating the onset-transient inhibition (i.e., fast recurrent inhibition), due to short-term depression (STD) at pyramidal cell (PC) to FS cell (PC-FS) synapses in response to a burst of PC action potentials (APs) (Pouille and Scanziani, 2004; Silberberg, 2008; Silberberg and Markram, 2007). In contrast, somatostatin (SST)-positive Martinotti cells (MCs) mediate the late-persistent inhibition (i.e., slow recurrent inhibition) resulting from short-term facilitation (STF) at PC-MC synapses (Blackman et al., 2013; Kapfer et al., 2007; Pouille and Scanziani, 2004; Silberberg, 2008; Silberberg and Markram, 2007; Zhu et al., 2011). In comparison with FS cells that discharge precisely at the onset of PC burst, MCs discharge persistently but with less temporal precision at late phase of PC burst (Pouille and Scanziani, 2004; Rozov et al., 2001). Interestingly, MC APs often outlast the presynaptic PC burst (Kapfer et al., 2007; Silberberg and Markram, 2007). The delayed firing in MCs and the resultant slow recurrent inhibition in neighboring PCs could be attributed to the overwhelming STF and the relatively slow membrane time constant of MCs (Kapfer et al., 2007; Pouille and Scanziani, 2004; Silberberg and Markram, 2007). However, it remains unclear what determines the AP precision and long-lasting firing in MCs.

In response to trains of presynaptic APs, both synchronous release (SR) and asynchronous release (AR) of neurotransmitters would occur in certain types of synapses, including GABAergic (Daw et al., 2009; Hefft and Jonas, 2005; Jiang et al., 2012, 2015; Lu and Trussell, 2000; Manseau et al., 2010) and glutamatergic synapses (Beierlein et al., 2003; Evstratova et al., 2014; Iremonger and Bains, 2007; Luo and Südhof, 2017). Unlike SR, AR is not tightly coupled to individual presynaptic APs. At GABAergic synapses, the occurrence of AR provides long-lasting inhibition to the postsynaptic cells, resulting in a reduction in their spiking probability and precision and thus a decrease in their

synchronization (Best and Regehr, 2009; Hefft and Jonas, 2005; Manseau et al., 2010). However, the occurrence of AR in glutamatergic synapses enhances and prolongs the postsynaptic spiking activities (Iremonger and Bains, 2007) and promotes the temporal precision of APs (Evstratova et al., 2014; Luo and Südhof, 2017). Recent studies revealed that the slow Ca^{2+} sensor synaptotagmin-7 (Syt7) plays an important role in both STF and asynchronous neurotransmitter release (Chen et al., 2017; Jackman et al., 2016; Luo and Südhof, 2017; Turecek and Regehr, 2018). Thus, it is of interest to examine whether the glutamatergic AR occurs at PC-MC synapses with STF and regulates spiking activities in MCs and the resultant inhibition, and whether AR is dependent on the identity of pre- or postsynaptic cells.

We performed dual whole-cell recordings from two PCs or PC and nearby interneurons in layer 5 of rodent somatosensory cortex (SSC). We found that glutamate AR occurs at PC output synapses in a target-cell-specific manner, with PC-MC pairs showing the strongest AR as compared with PC-PC and PC-FS pairs. In addition, AR is also dependent on presynaptic PC subtype; PCs projecting to dorsal striatum produce the strongest AR, as compared with those projecting to the pontine nuclei and the contralateral SSC. Glutamate AR from PC increases the neuronal excitability, prolongs AP firing, and reduces AP temporal precision of postsynaptic MCs. Thus, neighboring PCs receive long-lasting and desynchronized inhibitory postsynaptic potentials (IPSPs). We further demonstrate that glutamate AR depends on presynaptic Ca^{2+} level and Ca^{2+} sensor Syt7. Therefore, glutamate AR is a unique physiological property of PC-MC synapses and contributes to the regulation of cortical inhibition and information processing.

RESULTS

Desynchronized and Prolonged Slow Recurrent Inhibition and MC Firing

We performed dual whole-cell recordings from two neighboring PCs in layer 5 of rat SSC slices (Figure 1A). Approximately 26% of the PC-PC pairs (n = 29/113) showed slow disynaptic IPSPs in response to presynaptic AP bursts (15–30 APs at 100–200 Hz). Pairs with fast disynaptic IPSPs were rare (<1%, n = 7/1,216 pairs) (Kapfer et al., 2007; Silberberg and Markram, 2007; Zhu et al., 2011). In agreement with the role of glutamatergic synapses from PC to interneurons, the slow disynaptic IPSPs could be completely blocked by 10 μM CNQX (6-cyano-7-nitroquinoxaline-2,3-dione, n = 4). Interestingly, the onset-latency jitter of slow disynaptic IPSPs (PC burst with 15 APs at 100 Hz) was 3 times greater than that of the fast disynaptic IPSPs (±2.86 versus ±0.96 ms, n = 8 versus n = 3) (Figure 1B). Surprisingly, individual IPSPs could be frequently observed long after the cessation of the train stimulation (mean ± SD: 83.1 ± 35.3 ms, n = 18) (Figures 1A and 1C).

The fast and the slow disynaptic IPSPs could be mediated by FS basket cells and MCs, respectively (Blackman et al., 2013; Silberberg, 2008). As suggested by previous findings (Kapfer et al., 2007; Pouille and Scanziani, 2004), the large jitter of the slow disynaptic IPSPs could be attributed to the firing properties of MCs. We therefore performed dual whole-cell recordings from monosynaptically connected PC-MC pairs (Figure 1D). Putative MCs were identified by their vertically positioned spindle-shaped somata under IR-DIC microscope together with distinct electrophysiological properties, including a low-threshold spiking and/or an adapting pattern (Nigro et al., 2018; Otsuka and Kawaguchi, 2009; Wang et al., 2004) (Figure S1). Post hoc staining revealed that 98% of the recorded cells expressed SST (n = 39/40; Figure 1D). Three-dimensional reconstruction of the recorded pairs showed that all the postsynaptic cells possessed axon collaterals ascending to layer 1 and bitufted dendrites (n = 15/15; see below), characteristic morphology of MCs. We changed the presynaptic AP number from 15 to 30 to increase the possibility of MC firing at a membrane potential (V_m) of −60 mV (9.9%, n = 30/302 pairs). In 16 out of 20 recorded PC-MC pairs, APs in MCs could outlast the train stimulation (Figure 1E). The last post-train AP (PT-AP) occurred 55.4 ms after the train (range from 2.7 to 187.6 ms, n = 16). In agreement with the variability of individual slow disynaptic IPSPs, the jitter of intra-train APs (IT-APs) was large (±2.64 ms, n = 19) (Figure 1F). Since the jitter of inhibitory postsynaptic current (IPSC) onset latency in monosynaptically connected MC-PC pairs was very small (±0.44 ms, n = 4), we conclude that the jitter of disynaptic IPSCs (Figure 1B) is largely determined by the spike timing of MCs. Optogenetic inhibition of SST cells in mouse slices abolished disynaptic IPSPs (PC-PC pairs from $SST^{Cre}xAi35^{Arch\text{-}GFP}$ mice, n = 5) (Figure S2), further supporting a role of SST-positive MCs in mediating the slow disynaptic inhibition.

With extracellular stimulation (30 pulses at 100 Hz), we were able to compare the variability of APs in FS cells and putative MCs. In cell-attached configuration with stimulus intensity of 80 μA, MCs discharged APs with a jitter of ±1.51 ms (n = 6), substantially larger than FS cells (±0.84 ms, n = 6, p = 0.006, two-sample Student's t test) (Figures S3A and S3B). Similar results were obtained from whole-cell recordings (MCs, ±1.76 ms versus FS cells, ±0.78 ms, n = 16 versus n = 8, $p = 2.84 \times 10^{-6}$, two-sample Student's t test) (Figures S3C and S3D). To examine whether the spike precision depends on the strength of synaptic inputs, we varied the stimulus intensity from 40 to 120 μA for MCs and 60 to 100 μA for FS cells to reach their AP threshold but avoid direct axon stimulation. The AP jitter in MCs progressively decreased with increasing stimulus strength, but was significantly greater than that of FS cells at intensities tested (MCs: n = 11 versus FS cells: n = 8, $p = 2.55 \times 10^{-6}$, two-way ANOVA) (Figure S3E). Moreover, the jitter of MC (but not FS cell) APs progressively increased during the train stimulation (Figure S3F). The PT-AP could be frequently observed (n = 16/18 MCs) and outlasted the train by 90.2 ms (range from 42.2 to 210.3 ms, n = 16) (Figure S3G). Depolarization of the MCs would further prolong the average time window of post-train firing (from 46.5 to 96.0 ms, n = 6) (Figure S3G).

Together, our results demonstrate that, unlike FS cells, MCs discharge with less precision and APs often outlast the burst firing of the presynaptic PC, thus producing long-lasting inhibition with less precision in neighboring PCs.

Asynchronous Release Occurs at PC Synapses onto MCs

Close examination of the excitatory postsynaptic potentials or currents (EPSPs or EPSCs) in putative MCs reveals that, in

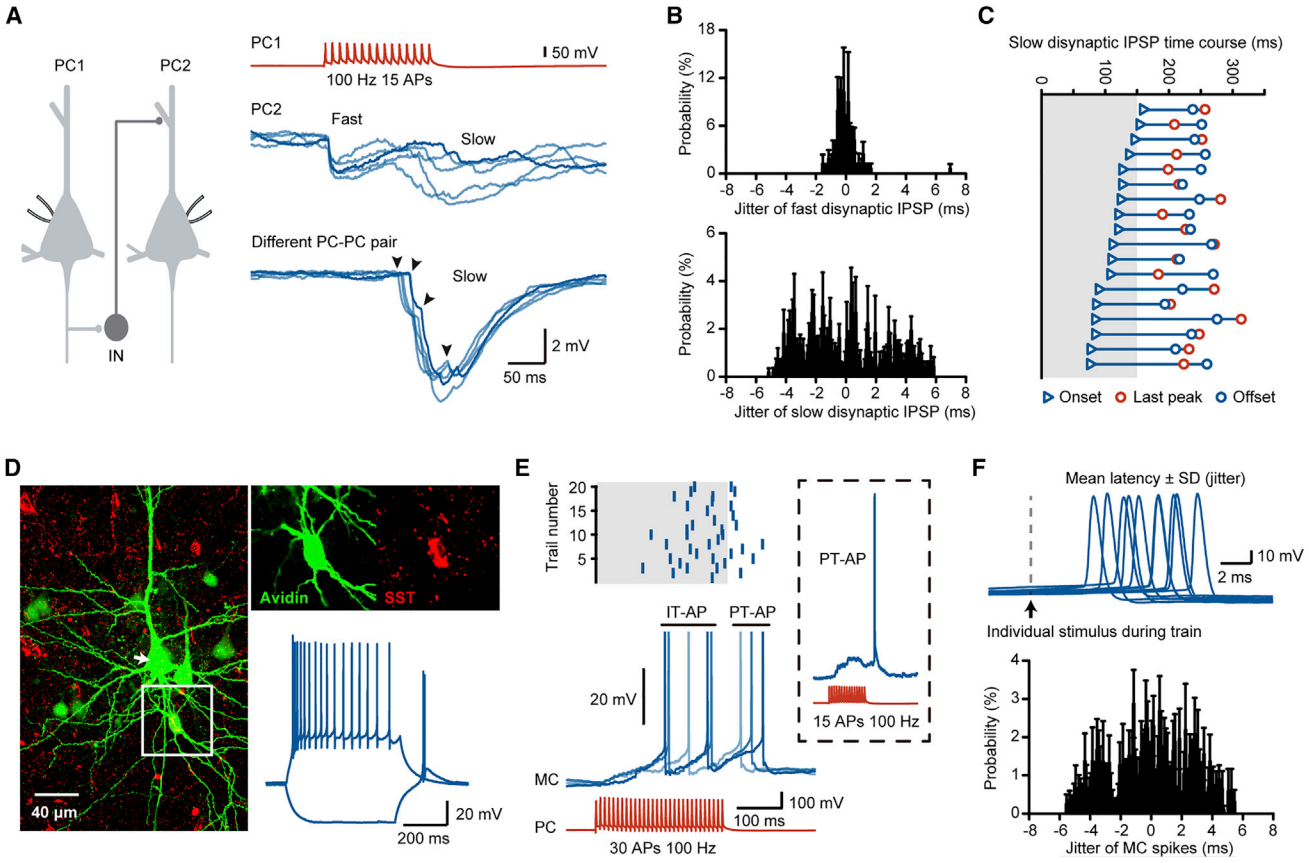

Figure 1. Desynchronized and Prolonged Slow Recurrent Inhibition and MC Firing

(A) Simultaneous whole-cell recording from a layer 5 PC-PC pair with disynaptic IPSPs. A train of stimulation in the presynaptic PC1 evokes both fast and slow disynaptic IPSPs in the postsynaptic PC2 (top). Another example (bottom) shows the occurrence of slow disynaptic IPSPs only. Note the individual IPSPs (arrowheads).

(B) Jitter of the onset latency of individual IPSPs (bin width: 0.1 ms; the abscissa shows the difference between each onset latency and the mean after a given pulse in presynaptic PC).

(C) Time course of slow disynaptic IPSPs. Blue, average disynaptic IPSP onset (triangles) and offset (circles); red circles, the last peak of IPSP event among all trails. The shadow indicates the period of train stimulation.

(D) Left, post hoc staining of a pair with synaptic connection from the PC (arrow) to the SST-positive MC. Right top, single images showing the cell is positive to both avidin and SST; bottom, firing pattern of the SST-positive cell.

(E) Bottom, a representative recording from a synaptically connected PC-MC pair. A train of PC stimulation induces repetitive MC firing, including intra-train (IT) and post-train (PT) APs (truncated). Top, raster plot of MC APs during (shadow) and after the train stimulation. Inset, PT-AP could be also observed in response to 15 APs at 100 Hz stimulation.

(F) Top, 10 superimposed APs (from the MC in E) showing the variation of AP latency. APs are aligned to their immediate preceding stimulus (arrow and dashed line) during the train. Bottom, the jitter of the MC spike latency (bin width: 0.1 ms).

Data are mean ± SEM. See also Figures S1–S3.

addition to SR (latency: 1.14 ± 0.19 ms, n = 10), barrages of asynchronous synaptic events that are not tightly coupled to presynaptic APs occur during and after the PC burst (Figure 2A). These events could be completely blocked by 10 μM CNQX (n = 5) (Figure 2B). To exclude the possibility that AR is due to whole-cell recording with membrane rupture, we performed loose-patch stimulation in the presynaptic PC and found robust AR in response to both low- and high-frequency stimulation (n = 7) (Figure 2C).

Two pieces of evidence indicate that the asynchronous synaptic events are monosynaptic AR from PC to MC, rather than polysynaptic transmission. One is that they only occur in monosynaptically connected PC-MC pairs (n = 302). If PC bursts evoke polysynaptic transmission via the activation of other excitatory neurons, the asynchronous events should be detected in both monosynaptically connected and unconnected PC-MC pairs. However, among 22 unconnected pairs, we found no obvious increase in the number of spontaneous EPSCs in response to 30-AP burst in a time window of 500 ms after the burst onset, even with a frequency up to 200 Hz (before: 2.16 ± 2.47 versus after: 2.23 ± 2.52 events, p = 0.74, Wilcoxon signed-rank test). The other evidence is that, among monosynaptically connected PC-PC pairs, none of them showed evoked postsynaptic AP in response to

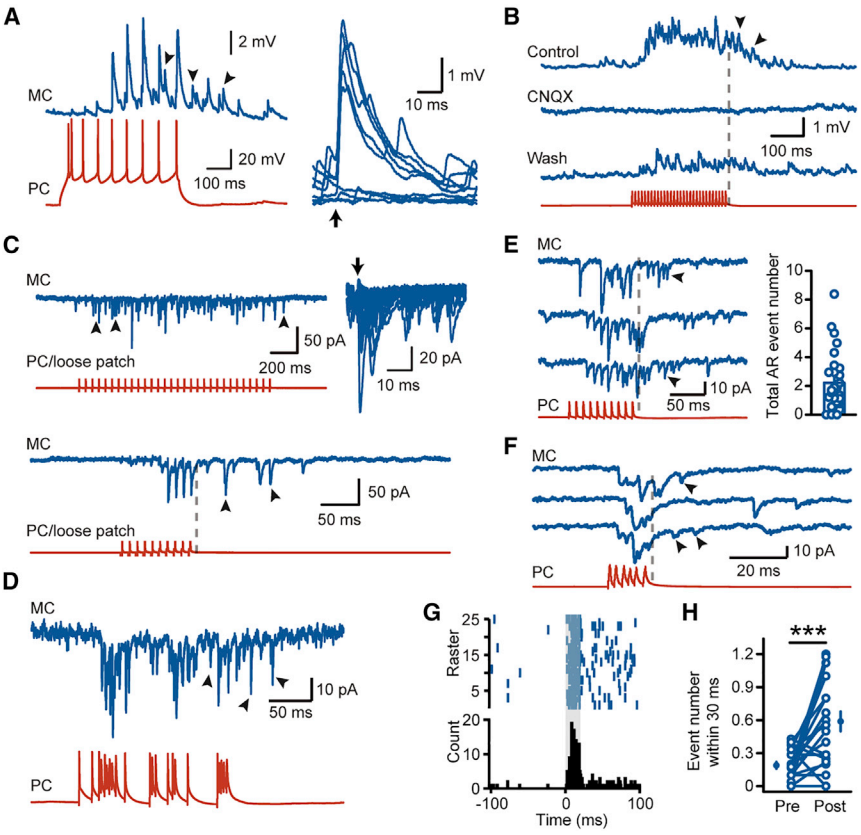

Figure 2. Asynchronous Glutamate Release Occurs at PC-MC Synapses

(A) A representative PC-MC pair recording. A burst of APs evoked by step current injection in PC (100 pA, red) induces facilitating EPSPs in the postsynaptic MC (blue). Arrowheads indicate AR events that are not tightly coupled to the presynaptic APs. Right, superimposed EPSPs aligned to the time of PC APs (arrow).

(B) Both SR and AR events could be blocked by the bath application of 10 μM CNQX. Arrowheads indicate AR events. Dotted line indicates the time when the train stimulation stops.

(C) Examples showing whole-cell recording in MC but loose-patch stimulation in PC (top, 30 pulses at 20 Hz; bottom, 10 pulses at 100 Hz). Top right, superimposed EPSCs aligned to individual stimulation pulses (30 pulses at 20 Hz). Arrow indicates the time of stimulation. Arrowheads indicate example AR events.

(D) An example PC-MC pair showing the occurrence of AR in response to a train of APs with Up-state spike timing (Figure S5B). Arrowheads indicate AR events.

(E) AR occurs in the ACSF with lower Ca^{2+} and Mg^{2+} (1.2 mM Ca^{2+} and 1 mM Mg^{2+}). Left, three example current responses in MC (blue) to PC train stimulation (red, 10 APs at 100 Hz) are shown. Arrowheads indicate AR events. Right, group data showing the total AR event number in different PC-MC pairs.

(F) Same pair as in (E). AR also occurs in response to PC burst with spike timing similar to that during synaptic stimulation in cell-attached recording. Arrowheads indicate AR events.

(G) Top, raster plot of EPSC events occurred in the MC before, during (shadow), and after the PC bursts. Bottom, histogram of the events (bin width: 1 ms).

(H) Group data showing the event number within 30 ms before and after the burst. Paired Student's t test, ***$p < 0.001$.

Data are mean ± SEM. See also Figures S4–S6.

presynaptic bursts, due to their weak unitary EPSPs (1.96 ± 1.15 mV, n = 22) and STD.

Next, we examined the occurrence of AR in physiological conditions and compared the AR strength (i.e., event number, charge, and basal current) (Figure S4). We stimulated the presynaptic PC with similar spike timing to that during the Up state in anaesthetized rat (see STAR Methods) and observed robust AR that could outlast the PC burst with post-train AR (PT-AR) duration of 87.1 ± 46.2 ms (n = 7) (Figures 2D and S5A–S5C). AR also occurred when Ca^{2+} and Mg^{2+} were reduced to a more physiological concentration (1.2 mM Ca^{2+} and 1 mM Mg^{2+}) (Ding et al., 2016; Sanchez-Vives and McCormick, 2000) and the number of presynaptic APs during the 100 Hz train stimulation was reduced to 10; the average total AR event number was 2.21 ± 2.03 (n = 29) (Figure 2E). Previous cell-attached recordings showed that layer 5 PCs in rat somatosensory cortex could generate spike bursts consisting of up to 5–6 APs (>100 Hz) in cortical slices (Williams and Stuart, 1999) and in awake animals (de Kock and Sakmann, 2008). We thus evoked bursts of 6 APs in presynaptic PCs with similar inter-spike intervals (ISIs: 2.72, 3.46, 2.72, 2.69, and 3.92 ms) to that in cell-attached recordings (Williams and Stuart, 1999) (Figure 2F) and revealed an increase in the number of spontaneous EPSCs (Figure 2G), attributed to the generation of AR events. The average event number 30 ms after the burst cessation showed a 2-fold increase from the baseline 0.19 ± 0.14 to 0.59 ± 0.41 (n = 21, $p = 6.84 \times 10^{-4}$, paired Student's t test) (Figure 2H). In experiments with further reduction of Ca^{2+} concentration to 1 mM (n = 6), we still observed the occurrence of AR, although the AR strength was weaker than that in 2 mM Ca^{2+}/Mg^{2+} ACSF (n = 10), possibly due to a reduction in release probability (Figure S5D) (Miki et al., 2018). These results indicate that AR occurs at PC output synapses onto MCs under physiological conditions.

Similar to GABAergic synapses (Hefft and Jonas, 2005; Jiang et al., 2012), PC-MC synapses also show dependence of AR strength on the number and frequency of presynaptic APs. Increasing the number or the frequency of APs would substantially increase the AR strength (n = 13) (Figure S6).

Glutamate AR Enhances MC Firing but Reduces AP Precision

We next compared spiking activities in putative MCs with and without AR. To reduce AR strength, we filled the patch pipette with an internal solution containing the Ca^{2+} chelator EGTA (10 mM). Consistent with previous studies (Goda and Stevens, 1994; Hefft and Jonas, 2005; Manseau et al., 2010), EGTA could progressively and dramatically reduce AR events, charge, and

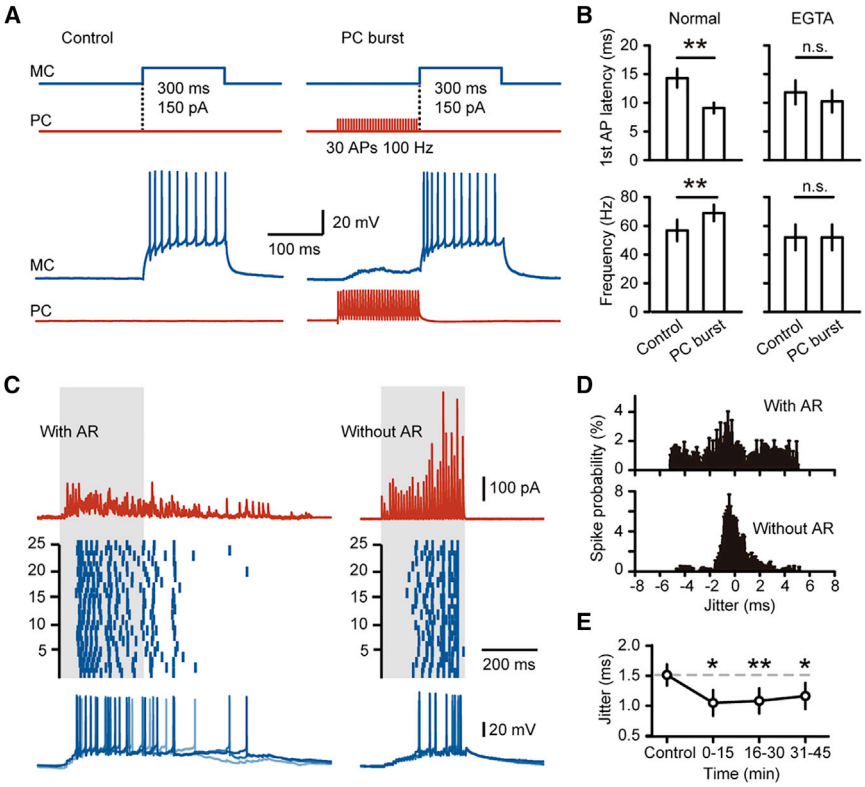

Figure 3. AR Increases Responsiveness of MCs but Reduces AP Precision

(A) Top, diagrams show experimental protocols with and without train stimulation in PC. Bottom, representative recordings from a synaptically connected PC-MC pair.

(B) Group data of the onset latency of the first AP (top) and the frequency during the initial 50 ms (bottom) in response to the step current injection. EGTA, 10 mM in pipette solution for PC recording.

(C) Example V_m responses (blue) to the injection of EPSC-like currents with (top left) and without AR (top right). Middle, raster plots of the APs. The total charge during the train (shadow) is similar in the two conditions.

(D) Jitter of the latency of each AP to its immediate preceding stimulus. Top, injection of an identical AR-containing EPSC-like current. Bottom, injection of an identical EPSC-like current without AR.

(E) Time course of the jitter of last 10 APs in MCs evoked by extracellular stimulation (30 stimuli at 100 Hz) with the application of 200 μM EGTA-AM. Data are mean ± SEM. Paired Student's t test, *$p < 0.05$; **$p < 0.01$; n.s., not significant. See also Figures S7–S8.

basal current (n = 9) (Figure S7). In contrast, the effect of EGTA on SR was relatively weaker (Figures S7C and S7D).

We first examined the effect of PT-AR on the responsiveness of MCs by measuring the latency of the first AP and the initial 50 ms firing frequency in response to a 150 pA pulse (Figure 3A). These current pulses were delivered to MCs immediately after the cessation of PC stimulation. In comparison with trials without PC stimulation (i.e., no synaptic transmission), those with 100 Hz 30-AP stimulation showed a reduction in the latency of the first AP in MCs by 36% (14.3 ± 4.9 versus 9.1 ± 2.8 ms, n = 9, p = 0.004, paired Student's t test) and an increase in firing frequency by 21% (56.8 ± 22.2 versus 69.0 ± 16.9 Hz, p = 0.005, paired Student's t test) (Figure 3B). However, with 10 mM EGTA in presynaptic PC, no significant difference could be detected in the latency of the first AP (11.8 ± 5.1 versus 10.3 ± 4.7 ms, n = 6) and the frequency of MC firing (52.0 ± 21.9 versus 52.0 ± 21.9 Hz) (Figure 3B). These results indicate that PT-AR increases neuronal responsiveness in MCs.

We next examined the effect of intra-train AR (IT-AR) on spike timing of MCs. Since presynaptic EGTA would dramatically reduce the depolarization and thus firing in MCs, we chose to evoke APs in MCs by injecting scaled EPSC-like currents (Figures 3C and S8A). Currents containing AR were obtained from a PC-MC pair recorded with normal pipette solution, whereas those without AR were obtained by re-patching the presynaptic PC with a pipette solution containing 10 mM EGTA. The synaptic currents without AR were then scaled to an extent that could evoke similar number of APs during the train (5.14 ± 1.84) to those with AR (4.85 ± 2.32, n = 7) (Figure S8B). The jitter of APs evoked by the same AR-containing EPSC-like current was ±2.73 ms (Figure 3D), consistent with the large jitter of MC IT-APs (Figure 1F). In sharp contrast, the jitter reduced to ±1.23 ms when the EPSC-like current contained no AR (Figure 3D). Similar results were obtained in experiments with extracellular stimulation and 200 μM EGTA-AM in the bath. EGTA-AM significantly decreased the jitter of last 10 APs in MCs evoked by extracellular stimulation (30 stimuli at 100 Hz) from ±1.51 to ±1.08 ms (after 30 min drug application, n = 6, p = 0.007, paired Student's t test) (Figure 3E).

Previous studies reported that glutamate AR increased AP precision at synapses with strong unitary EPSCs (Evstratova et al., 2014; Luo and Südhof, 2017). We then investigated whether synaptic strength affects AP timing using dynamic clamp to inject artificial synaptic conductances (α-synapse: τ = 1.64 ms). We found that a constant V_m depolarization decreases the jitter of APs evoked by a synaptic conductance of 8 nS, suggesting that AR-associated basal current would cause depolarization and enhance spike precision (n = 5) (Figures S8C and S8D). However, for the same cell at a similar V_m level (−55.4 ± 4.8 versus −55.5 ± 4.6 mV, n = 5), APs induced by a weaker synaptic input (4 nS) 40 ms after the extracellular stimulation showed less spike precision as compared to those evoked by the strong input (8 nS). The strong input decreased not only the failure rate but also the jitter from ±1.09 to ±0.40 ms ($p = 8.37 \times 10^{-4}$, paired Student's t test) (Figures S8E and S8F). Since the SR strength at PC-MC synapse is much smaller (1st EPSC amplitude: 4.9 ± 4.7 pA; the maximum amplitude during PC burst: 24.7 ± 15.8 pA, n = 73 pairs) than that at hippocampal mossy fiber or

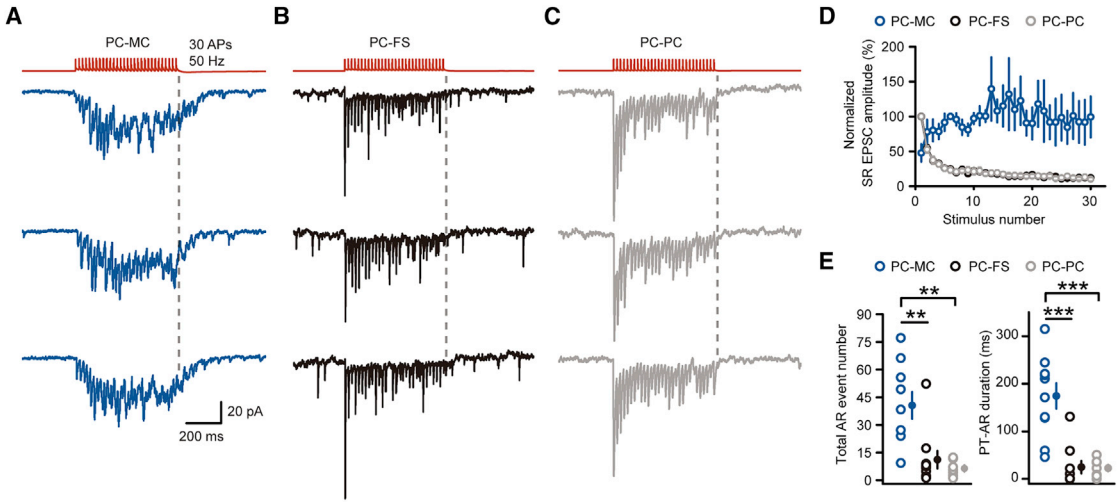

Figure 4. AR at Output Synapses of PC Is Target-Cell Specific

(A) Representative recordings from a PC-MC pair. Three current responses in MC (blue) to AP trains in PC (red) are shown. The dotted line indicates the cessation of the train. Note the occurrence of AR after the train.

(B) Recordings from a PC-FS pair.

(C) Recordings from a PC-PC pair.

(D) Time course of the peak amplitude of SR EPSCs. The amplitudes for PC-PC and PC-FS pairs (STD) are normalized to the 1st EPSC. The amplitudes for PC-MC pairs (STF) are normalized to the 6th EPSC because the initial EPSCs show a high failure rate.

(E) Group data showing total AR event number (left) and PT-AR duration (right) of PC-MC, PC-FS, and PC-PC pairs. Two-sample Student's t test, **$p < 0.01$; ***$p < 0.001$.

Data are mean ± SEM. See also Figures S4 and S9.

Calyx of Held (Evstratova et al., 2014; Luo and Südhof, 2017), AR provides synaptic noise that would smooth out the V_m and elevate its level to AP threshold, resulting in desynchronized AP firing. Together, these results indicate that AR from PCs not only enhances neuronal responsiveness but also reduces the temporal precision of evoked APs in MCs.

AR Is Target-Cell Specific and PC-Subtype Dependent

Considering that PC forms synapses onto different types of neurons (Rozov et al., 2001), we next compared the AR strength of PC-MC to those of PC-FS and PC-PC (Figures 4A–4C). Similar to previous findings (Beierlein et al., 2003; Koester and Johnston, 2005; Pala and Petersen, 2015), our results reveal short-term facilitation in PC-MC, but depression in PC-FS and PC-PC pairs with presynaptic 50 Hz stimulation (Figure 4D). The total numbers of AR events in PC-MC, PC-FS, and PC-PC pairs were 40.6 ± 23.0, 11.1 ± 15.2, and 6.4 ± 4.3, respectively (PC-MC, n = 10; PC-FS, n = 10; PC-PC, n = 7) (Figure 4E). Dramatic differences were also found in the PT-AR duration (Figure 4E), the PT-AR charge ratio, and basal currents (Figure S9A). Consistently, similar differences were observed between PC-SST and PC-PV cell pairs in slices from transgenic mice ($SST^{Cre}xAi9^{tdTomato}$ mice, n = 7 versus $PV^{Cre}xAi9^{tdTomato}$ mice, n = 7) (Figure S9B). Moreover, AR strength is independent of cortical regions because the AR strength of PC-MC pairs in rat SSC and prefrontal cortex (PFC) slices showed no significant difference (SSC, n = 10; PFC, n = 7) (Figure S9C). These results indicate that AR at glutamatergic synapses is target-cell specific, and the strongest AR occurs at PC-MC synapses.

Recent studies reveal that MCs can be further subdivided into two subpopulations with fanning-out or T-shaped axon arborizations (Muñoz et al., 2017; Nigro et al., 2018). We therefore reconstructed 15 PC-MC pairs (Figures 5A and 5B) and compared their AR strength. Fanning-out MCs had a lower input resistance (120 ± 36 MΩ, n = 7) than T-shaped MCs (245 ± 94 MΩ, n = 8, p = 0.007, two-sample Student's t test) (Nigro et al., 2018). No significant difference in AR strength was detected between the two MC subgroups (Figure 5C). However, the parameters of T-shaped (but not fanning-out) MCs show a strong negative correlation with MC input resistance (Figure 5C), possibly resulting from a progressive decrease in release probability as reflected by an increase in failure rate (Figure 5D). Weak correlations were also found in much larger datasets of MCs including unreconstructed cells (n = 57) (Figures 5E and 5F).

Next, we examined whether the AR strength depends on presynaptic PC subtype. We injected retrograde beads to specific brain regions to label corticopontine (CPn), commissural (COM), and crossed-corticostriatal (CCS) PCs in SSC (Figures 6A–6C) (Hattox and Nelson, 2007; Kawaguchi, 2017). Surprisingly, we found that PC_{CCS}-MC pairs produce much stronger AR than PC_{CPn}-MC and PC_{COM}-MC pairs (PC_{CPn}-MC, n = 7; PC_{COM}-MC, n = 7; PC_{CCS}-MC, n = 9) (Figure 6D) and have a much lower failure rate (Figure 6E). The connection probability of PC_{CCS}-MC pairs (n = 9/16) was substantially higher than PC_{CPn}-MC (n = 7/46) and PC_{COM}-MC pairs (n = 7/45), and MCs receiving PC_{CCS}-PC inputs had a significantly lower input resistance (160 ± 58 MΩ versus 284 ± 108 MΩ in PC_{CPn}-MC pairs and 355 ± 143 MΩ in PC_{COM}-MC pairs, p = 0.03, one-way

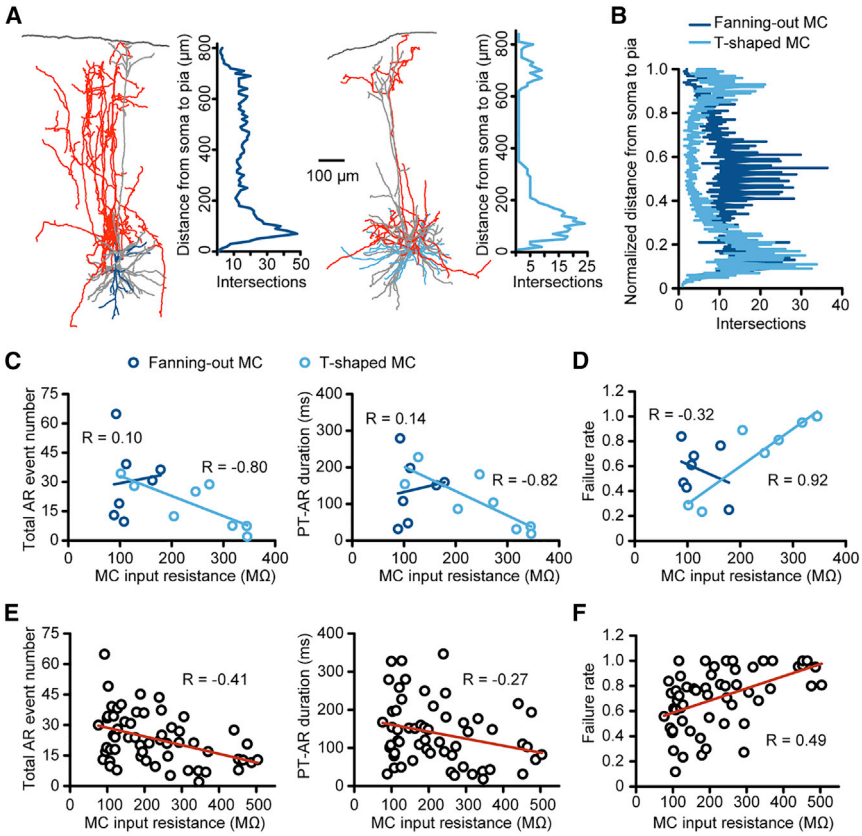

Figure 5. AR at PC Synapses onto MCs with Fanning-Out or T-Shaped Axon Arborization

(A) 3D reconstruction of two PC-MC pairs. Left, a PC and a fanning-out MC; right, a PC and a T-shaped MC. The axons of MCs were shown in red, and the dendrites in blue. PC dendrites were shown in gray. Insets, Sholl analysis of MC axons.

(B) Group data for Sholl analysis of MC axons.

(C) Plots of the total AR event number (left) and PT-AR duration (right) as a function of MC input resistance. Continued lines are linear regression fits of the corresponding datasets.

(D) Group data showing the correlation of MC input resistance with the failure rate of unitary EPSCs.

(E) Similar as in (C), but include unreconstructed MCs.

(F) Similar as in (D), but include unreconstructed MCs.

Data are mean ± SEM. See also Figure S4.

ANOVA) (Figure 6F). These results suggest that, in comparison with CPn and COM PCs, CCS PCs may cause longer-lasting firing in MCs and thus produce sustained inhibition in somatosensory cortical network.

Role of Syt7 in Regulating AR and Recurrent Inhibition

Recent studies revealed that the slow Ca^{2+} sensor, Syt7, plays important roles in regulating synaptic transmission, especially AR (Bacaj et al., 2013; Chen et al., 2017; Luo and Südhof, 2017; Turecek and Regehr, 2018; Wen et al., 2010). We therefore examined whether Syt7 could regulate AR at PC-MC synapses. Syt7 antibody staining showed a pattern in the cerebellum (Figures S10A–S10C) similar to previous reports (Chen et al., 2017; Turecek et al., 2017). We observed strong immunosignals in the SSC of wild-type (WT) mice, but not in Syt7 knockout (KO) mice (Figures 7A and S10A–S10C). Moreover, signals co-localized with vesicular glutamate transporter 1 (vGlut1) (Figure 7A), suggesting an expression of Syt7 at glutamatergic terminals in the neocortex.

We next examined the strength of AR in PC-MC pairs of WT and Syt7 KO mice (Figure 7B). The number of IT-AR events was significantly, but not completely, decreased in Syt7 KO mice (13.2 ± 8.7 versus 6.3 ± 4.6, n = 20 and 19, p = 0.018, Mann-Whitney *U* test) (Figure 7C). The PT-AR event number was also reduced, but not significantly (11.6 ± 12.3 versus 5.9 ± 8.1, p = 0.29, Mann-Whitney *U* test). The basal current was substantially decreased in KO mice (11.6 ± 6.4 versus 6.4 ± 5.3 pA, p = 0.003; Mann-Whitney *U* test) (Figure 7D). The remaining AR events could be further eliminated by the inclusion of 10 mM EGTA in the pipette solution (Figure S10D), suggesting the existence of another unknown Ca^{2+}-dependent mechanism underlying the occurrence of AR in addition to Syt7. In agreement with previous studies (Chen et al., 2017; Luo and Südhof, 2017; Turecek and Regehr, 2018), Syt7 deletion eliminated synaptic facilitation by reducing SR amplitudes and increasing failure rates during the train stimulation (Figure S10E), but it showed no effect on the amplitude of unitary EPSCs (WT, 6.17 ± 5.22 versus KO, 4.84 ± 4.11 pA, p = 0.58, Mann-Whitney *U* test) and the initial release probability as reflected by their failure rates (0.63 ± 0.27 versus 0.65 ± 0.27, p = 0.86, Mann-Whitney *U* test). The SR-associated charge in KO mice was decreased by ~41.6% (1.12 ± 0.74 versus 0.65 ± 0.62 pA·s, p = 0.004, Mann-Whitney *U* test), but to a lesser extent than that of the total AR charge (~50.4%, 2.93 ± 1.83 versus 1.46 ± 1.25 pA·s, p = 0.005, Mann-Whitney *U* test).

To investigate the role of Syt7 in the regulation of slow recurrent inhibition, we compared disynaptic IPSPs in WT and KO mice (Figure 7E). The onset of disynaptic IPSPs was significantly delayed in KO mice (222 ± 49 ms, n = 16) compared to in WT mice (174 ± 51 ms, n = 15, p = 0.01, two-sample Student's t test) (Figure 7F). The offset of disynaptic IPSPs showed no significant change (WT, 405 ± 45 versus KO, 428 ± 46 ms, p = 0.17, two-sample Student's t test). Accordingly, the symmetry ratio of the onset-to-peak time to peak-to-offset time (Berger et al., 2009) was significantly reduced in KO mice (0.41 versus 0.31, p = 0.004, two-sample Student's t test) (Figure 7F). At similar postsynaptic V_m levels (~ 51 mV), both the peak amplitude (WT, 4.54 ± 1.20, n = 8 versus KO, 3.28 ± 1.10 mV, n = 8, p = 0.047, two-sample Student's t test) and the voltage integral (0.58 ± 0.23 versus 0.34 ± 0.18 mV·s, p = 0.037, two-sample Student's t test) were significantly decreased in KO mice (Figure 7G), suggesting a decrease

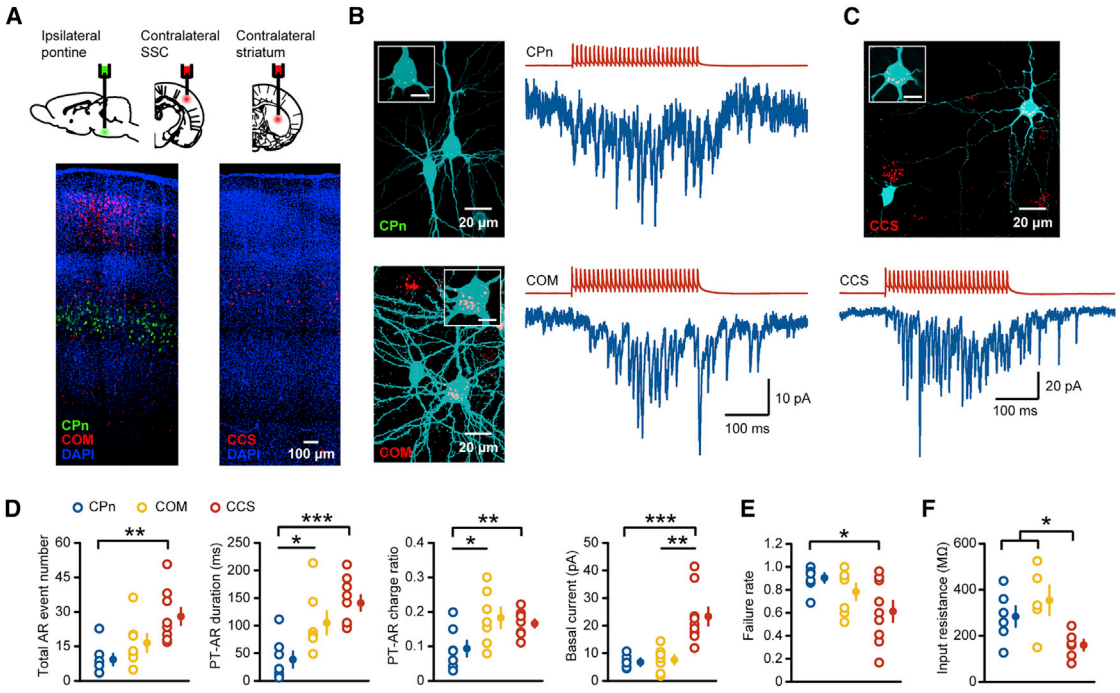

Figure 6. The Strength of AR Is Dependent on PC Subtypes

(A) Top, the injection sites of retrograde beads. Bottom, example SSC slices showing the retrograde beads in a subpopulation of cells. Ipsilateral pontine and contralateral SSC injections were performed in the same rat, whereas contralateral dorsal striatum injection was performed in different animals. These injections will label corticopontine (CPn), commissural (COM) and crossed-corticostriatal (CCS) PCs.

(B) Left, example cells with avidin staining and retrograde beads (top, PC_{CPn}-MC; bottom, PC_{COM}-MC); right, example recordings from pairs shown in the left. Insets, single images showing avidin-stained PCs containing beads, scale bar: 10 μm.

(C) Similar as in (B), but for a PC_{CCS}-MC pair.

(D) Comparison of the AR strength between different types of pairs.

(E) Group data showing differences in the failure rate of unitary EPSCs.

(F) Input resistance of MCs in different types of pairs.

Data are mean ± SEM. (D) and (E), two-sample Student's t test; (F), one-way ANOVA; *p < 0.05; **p < 0.01; ***p < 0.001. See also Figure S4.

in MC firing. The delayed onset and reduced disynaptic inhibition in Syt7 KO mice could be largely due to the reduction in AR and basal current. These results indicate that Syt7 contributes to the regulation of slow recurrent inhibition.

DISCUSSION

We demonstrate that, in response to PC bursts, MCs produce long-lasting and temporally imprecise APs, due to asynchronous glutamate release at PC-MC synapses. Interestingly, the strength of AR is not uniform at PC output synapses; AR at PC-MC synapses is much stronger than at PC-FS and PC-PC synapses. In addition, among PC-MC synapses, PC_{CCS}-MC pairs possess the strongest AR. We further reveal that AR depends on residual Ca^{2+} levels, and its strength depends on presynaptic AP number and frequency. The selective occurrence of AR at PC-MC synapses determines the timing and the size of slow recurrent inhibition received by neighboring PCs.

Selective Occurrence of AR at Certain Types of Synapses

Asynchronous neurotransmitter release has been found in both the periphery (Rahamimoff and Yaari, 1973) and central nervous system (Daw et al., 2009; Hefft and Jonas, 2005; Iremonger and Bains, 2007; Jiang et al., 2012; Lu and Trussell, 2000; Manseau et al., 2010), but it is only found at synapses onto or from certain types of neurons. In the hippocampus, granule cells receive much stronger AR of GABA from CCK-containing neurons than PV cells (Daw et al., 2009; Hefft and Jonas, 2005). In the neocortex, FS cells show stronger AR at their autapses than those onto PCs and other FS cells (Jiang et al., 2012). Our results indicate that AR also occurs at PC output synapses, and its strength is dependent on the cell type of both pre- and postsynaptic cells.

Why does AR selectively occur at certain types of synapses? In output synapses of FS cells, the Ca^{2+}-binding protein PV may act as a Ca^{2+} buffer and prevent the occurrence of AR (Eggermann and Jonas, 2011; Hefft and Jonas, 2005; Jiang et al., 2015; Manseau et al., 2010). Differences in voltage-gated Ca^{2+} channel subtypes and their distance to Ca^{2+} sensors at the release site may also determine the AR strength (Eggermann et al., 2011; Rozov et al., 2001; Wadel et al., 2007). Indeed, loose coupling between Ca^{2+} channel and sensor at output synapses of hippocampal CCK neurons results in strong asynchronous GABA release, as compared with that of PV cells (Hefft and Jonas, 2005). Consistent with the difference in AR strength,

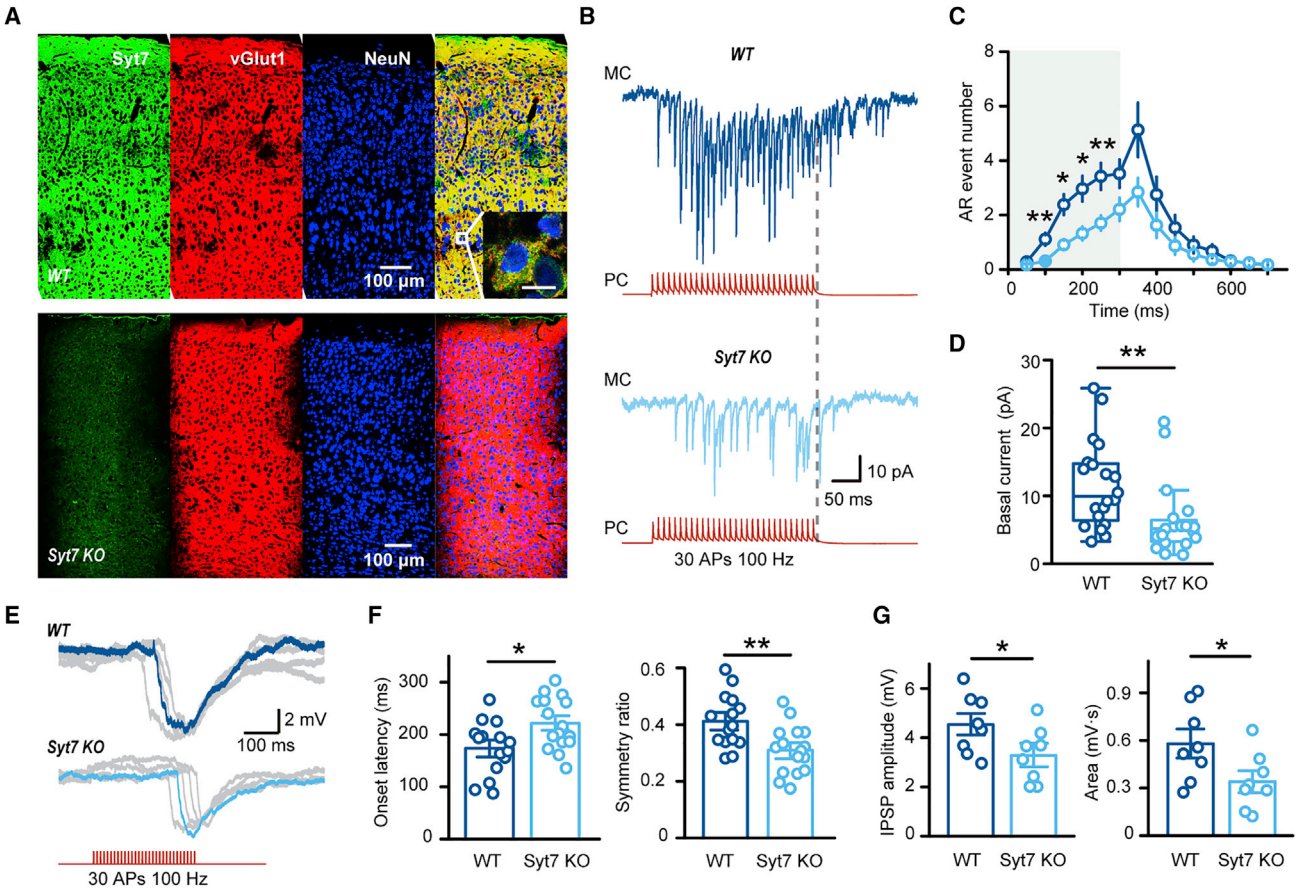

Figure 7. Syt7 Regulates AR at PC-MC Synapses and the Recurrent Inhibition

(A) Immunostaining of Syt7, vGlut1, and NeuN in SSC of WT and Syt7 KO mice. Inset, higher magnification showing the overlap of Syt7 and vGlut1 signals (scale bar: 10 μm).

(B) Two example recordings from PC-MC pairs of WT and KO mice.

(C) Time courses of the AR event number during (shadow) and after the train stimulation.

(D) Group data of the basal current.

(E) Representative disynaptic IPSPs from PC-PC pairs of WT and Syt7 KO mice. Superimposed individual sweeps are shown for each pair.

(F) Group data of the average onset latency and symmetry ratio of disynaptic IPSP barrages.

(G) Group data of the average peak amplitude and voltage integral (area) of disynaptic IPSP barrages.

Data are mean ± SEM for (C), (F), and (G), and median with 1.5× interquartile range for (D). Mann-Whitney *U* test for (C) and (D); two-sample Student's t test for (F) and (G). *p < 0.05; **p < 0.01. See also Figures S4 and S10.

channel-sensor distance at synapses of PC onto bipolar interneurons (presumably MCs) is greater than that of synapses onto multipolar interneurons (presumably FS cells) (Rozov et al., 2001).

AR and Short-Term Plasticity at PC-MC Synapses

PC-MC synapses possess a high failure rate, especially when PC fires at low frequencies (Koester and Johnston, 2005; Urban-Ciecko et al., 2018). In response to high-frequency PC burst, the release probability increases dramatically. This synaptic STF, together with the slow membrane constant, ensure MCs act as a high-pass filter in the neural network by generating late-persistent firing in response to high-frequency PC burst (Jonas et al., 2004; Kapfer et al., 2007; Silberberg, 2008; Silberberg and Markram, 2007; Urban-Ciecko and Barth, 2016). Our results reveal that AR occurs at late phases of the PC burst and even outlasts the burst, causing large and prolonged depolarization and thereby persistent firing in MCs. Therefore, AR is an important mechanism for MCs to work as a high-pass filter.

Previous studies reveal that AR is determined by the level of background or residual Ca^{2+} after the AP burst (Kaeser and Regehr, 2014), which is also closely related to the occurrence of STF (Chen et al., 2017; Turecek and Regehr, 2018). In our recordings, manipulation of Ca^{2+} level by reducing extracellular Ca^{2+} concentration or by including 10 mM EGTA in presynaptic pipette could decrease both AR and STF. Recent studies reveal the important role of the slow Ca^{2+} sensor Syt7 in regulating the occurrence of AR and STF (Chen et al., 2017; Jackman et al., 2016; Luo and Südhof, 2017; Turecek and Regehr, 2018). In subcortical regions and cerebellum, knocking out Syt7 has no

effect on the initial release probability and unitary synaptic strength, but it decreases the STF and the AR-mediated charge and basal current (Chen et al., 2017; Luo and Südhof, 2017; Turecek and Regehr, 2018), consequently causing a decrease in firing precision of postsynaptic neuron (Luo and Südhof, 2017). Similarly, our results indicate that Syt7 regulates both STF and AR during presynaptic AP bursts, but not the unitary EPSCs of PC-MC pairs in the neocortex. The reduction of AR is relatively greater than that of SR, which suggests a more important role of AR in regulating the slow recurrent inhibition; however, since the key mechanisms for SR and AR at presynaptic terminals may overlap (Kaeser and Regehr, 2014), it is difficult to isolate the two release modes completely. Considering that Syt7 KO could not block the AR events completely in our experiments, as well as those from others (Chen et al., 2017; Turecek and Regehr, 2018, 2019), we speculate that other Ca^{2+} sensors such as Doc2 (Yao et al., 2011) may also contribute to the occurrence of AR. However, the identity of these sensors and other functional molecules and their cooperation (Volynski and Krishnakumar, 2018) remains to be further examined.

Physiological Significance of AR at PC-MC Synapse

To the best of our knowledge, our results provide the first piece of evidence showing the effect of AR on the operation of cortical microcircuits. The glutamate AR from PC dramatically prolongs the time window of firing and desynchronizes APs in MCs, consequently causing long-lasting and relatively imprecise inhibition in the neighboring PCs, which will be smoothed out to form constant inhibition if a group of MCs are involved (Kapfer et al., 2007). Since MCs mainly send their axons to superficial cortical layers and target to the distal tuft dendrites of PCs (Urban-Ciecko and Barth, 2016; Wang et al., 2004), the constant inhibition provided by MCs could prevent the generation of broad dendritic Ca^{2+} spikes (Chiu et al., 2013; Murayama et al., 2009) and thereby suppress the burst firing in PCs (Gentet et al., 2012; Neske and Connors, 2016; Urban-Ciecko and Barth, 2016), resulting in a shift of their firing pattern and possibly an alteration in their synchronization that is critical for network oscillations.

Previous studies reveal a weak negative correlation between cortical SST and PC V_m fluctuations during quiet wakefulness (Gentet et al., 2012) and an important role of SST neurons in the control of state transitions (Up and Down states) during slow-wave oscillation (Zucca et al., 2017). Delayed and prolonged firing into the Down state in SST cells may help the network switch from Up to Down state. However, it remains unknown what drives SST cells to fire during the Down states. Our results indicate that glutamate AR from PC to SST-positive MC contributes to the generation of long-lasting depolarization and discharges outlasting PC activity. The lack of AR or weak AR at PC-PC and PC-FS pairs also explains well why V_m fluctuations of PCs and FS cells are highly and positively correlated (Gentet et al., 2012). Interestingly, intrinsically bursting PCs discharge more bursts during slow-wave sleep compared to other behavioral states (Steriade et al., 2001), and the extracellular Ca^{2+} concentration is substantially increased during sleep (Ding et al., 2016). The enhanced AR strength in these conditions may promote slow-wave sleep. Considering that slender-tufted PCs in layer 5A, presumably CCS PCs, become active during active whisking, whereas thick-tufted PCs respond to passive whisker touch (de Kock and Sakmann, 2009; Oberlaender et al., 2011), we speculate that the strong AR at PC_{CCS}-MC synapses would cause prolonged firing in MCs and long-lasting lateral inhibition during active whisking.

PCs in the neocortex normally generate APs at a frequency lower than 20 Hz *in vivo*, but they can also produce bursts with frequencies higher than 100 Hz (de Kock and Sakmann, 2008; Steriade et al., 1998, 2001; Yu et al., 2019). Sharp electrode intracellular recording revealed burst firing and high frequency firing in both intrinsically bursting PCs and regular-spiking cells during sleep (Steriade et al., 2001). In cell-attached recording both *in vitro* (Williams and Stuart, 1999) and in awake animals (de Kock and Sakmann, 2008), layer 5 PCs in the rat somatosensory cortex could generate spike bursts consisting of up to 5–6 APs at frequencies higher than 100 Hz. In our experiments mimicking physiological conditions by lowering the extracellular concentration of divalent cations (Ding et al., 2016) and producing burst of 6 APs with similar spike timing to cell-attached recording (Williams and Stuart, 1999), we still observed a dramatic increase in spontaneous EPSCs after the burst (Figures 2F–2H), indicating the occurrence of delayed AR. Although high-intensity stimulations (30 pulses at 100 Hz) were used to induce PC bursts in most of our experiments, we also found that AR occurred when the number of pulses was decreased and the frequency was lowered to 10–20 Hz (Figure 2). The dependence of AR on PC activity (Figure S6) may contribute to cortical excitation-inhibition balance, which is important for proper brain functions. In some pathological conditions such as epileptic seizures, PCs could generate high-frequency bursts lasting for tens of seconds or even minutes (Kawaguchi, 2001). The AR strength is also subject to change under pathological situations. In epileptic human neocortical tissue, AR becomes stronger at output synapses of FS cells (Jiang et al., 2012). At the neuromuscular junction, AR is also enhanced in mouse models of spinal muscular atrophy (Ruiz et al., 2010) and Alzheimer's disease (Yang et al., 2007). Whether the strength of glutamate AR and MC firing are subject to alteration in diseased states remains to be further examined.

Together, our results suggest an important physiological role of asynchronous glutamate release at PC output synapses in regulating the operation of cortical microcircuits. MCs receive AR during and after PC burst and generate late-persistent AP firing with less precision, which may produce long-lasting and desynchronized inhibition in nearby PCs that could be essential for efficient suppression of Ca^{2+} spikes in PC dendrites and control of cortical state transitions. Therefore, the selective occurrence of AR at PC-MC synapses exactly meets the need of information processing mediated by MCs in neocortical networks.

STAR★METHODS

Detailed methods are provided in the online version of this paper and include the following:

- KEY RESOURCES TABLE
- LEAD CONTACT AND MATERIALS AVAILABILITY
- EXPERIMENTAL MODEL AND SUBJECT DETAILS

SUPPLEMENTAL INFORMATION

Supplemental Information can be found online at https://doi.org/10.1016/j.neuron.2019.10.038.

ACKNOWLEDGMENTS

We are grateful to Drs. Z. Josh Huang (Cold Spring Harbor Laboratory), Hongkui Zeng (Allen Institute), and Thomas C. Südhof (Stanford University) for providing the transgenic mice. This work was supported by the National Natural Science Foundation of China (31430038, 31630029, and 31661143037).

AUTHOR CONTRIBUTIONS

S.D., J.L., and J.Z. performed the slice experiments. S.D. and J.L. performed the immunohistochemistry experiments. X.Y. performed the *in vivo* experiments. X.Z. and Z.M. helped with the experiments using Syt7 KO and WT mice. S.D., Q.H., J.L., L.L., M.J., Q.D., Y.M., and Y.S. analyzed the data. Y.S. and S.D. wrote the manuscript.

DECLARATION OF INTERESTS

The authors declare no competing interests.

Received: October 25, 2018
Revised: June 11, 2019
Accepted: October 28, 2019
Published: December 2, 2019

REFERENCES

Bacaj, T., Wu, D., Yang, X., Morishita, W., Zhou, P., Xu, W., Malenka, R.C., and Südhof, T.C. (2013). Synaptotagmin-1 and synaptotagmin-7 trigger synchronous and asynchronous phases of neurotransmitter release. Neuron *80*, 947–959.

Beierlein, M., Gibson, J.R., and Connors, B.W. (2003). Two dynamically distinct inhibitory networks in layer 4 of the neocortex. J. Neurophysiol. *90*, 2987–3000.

Berger, T.K., Perin, R., Silberberg, G., and Markram, H. (2009). Frequency-dependent disynaptic inhibition in the pyramidal network: a ubiquitous pathway in the developing rat neocortex. J. Physiol. *587*, 5411–5425.

Best, A.R., and Regehr, W.G. (2009). Inhibitory regulation of electrically coupled neurons in the inferior olive is mediated by asynchronous release of GABA. Neuron *62*, 555–565.

Blackman, A.V., Abrahamsson, T., Costa, R.P., Lalanne, T., and Sjöström, P.J. (2013). Target-cell-specific short-term plasticity in local circuits. Front. Synaptic Neurosci. *5*, 11.

Chen, C., Satterfield, R., Young, S.M., Jr., and Jonas, P. (2017). Triple Function of Synaptotagmin 7 Ensures Efficiency of High-Frequency Transmission at Central GABAergic Synapses. Cell Rep. *21*, 2082–2089.

Chiu, C.Q., Lur, G., Morse, T.M., Carnevale, N.T., Ellis-Davies, G.C., and Higley, M.J. (2013). Compartmentalization of GABAergic inhibition by dendritic spines. Science *340*, 759–762.

Daw, M.I., Tricoire, L., Erdelyi, F., Szabo, G., and McBain, C.J. (2009). Asynchronous transmitter release from cholecystokinin-containing inhibitory interneurons is widespread and target-cell independent. J. Neurosci. *29*, 11112–11122.

de Kock, C.P., and Sakmann, B. (2008). High frequency action potential bursts (>or= 100 Hz) in L2/3 and L5B thick tufted neurons in anaesthetized and awake rat primary somatosensory cortex. J. Physiol. *586*, 3353–3364.

de Kock, C.P., and Sakmann, B. (2009). Spiking in primary somatosensory cortex during natural whisking in awake head-restrained rats is cell-type specific. Proc. Natl. Acad. Sci. USA *106*, 16446–16450.

Ding, F., O'Donnell, J., Xu, Q., Kang, N., Goldman, N., and Nedergaard, M. (2016). Changes in the composition of brain interstitial ions control the sleep-wake cycle. Science *352*, 550–555.

Eggermann, E., and Jonas, P. (2011). How the 'slow' Ca(2+) buffer parvalbumin affects transmitter release in nanodomain-coupling regimes. Nat. Neurosci. *15*, 20–22.

Eggermann, E., Bucurenciu, I., Goswami, S.P., and Jonas, P. (2011). Nanodomain coupling between Ca^{2+} channels and sensors of exocytosis at fast mammalian synapses. Nat. Rev. Neurosci. *13*, 7–21.

Evstratova, A., Chamberland, S., Faundez, V., and Tóth, K. (2014). Vesicles derived via AP-3-dependent recycling contribute to asynchronous release and influence information transfer. Nat. Commun. *5*, 5530.

Gentet, L.J., Kremer, Y., Taniguchi, H., Huang, Z.J., Staiger, J.F., and Petersen, C.C.H. (2012). Unique functional properties of somatostatin-expressing GABAergic neurons in mouse barrel cortex. Nat. Neurosci. *15*, 607–612.

Goda, Y., and Stevens, C.F. (1994). Two components of transmitter release at a central synapse. Proc. Natl. Acad. Sci. USA *91*, 12942–12946.

Hattox, A.M., and Nelson, S.B. (2007). Layer V neurons in mouse cortex projecting to different targets have distinct physiological properties. J. Neurophysiol. *98*, 3330–3340.

Hefft, S., and Jonas, P. (2005). Asynchronous GABA release generates long-lasting inhibition at a hippocampal interneuron-principal neuron synapse. Nat. Neurosci. *8*, 1319–1328.

Iremonger, K.J., and Bains, J.S. (2007). Integration of asynchronously released quanta prolongs the postsynaptic spike window. J. Neurosci. *27*, 6684–6691.

Jackman, S.L., Turecek, J., Belinsky, J.E., and Regehr, W.G. (2016). The calcium sensor synaptotagmin 7 is required for synaptic facilitation. Nature *529*, 88–91.

Jiang, M., Zhu, J., Liu, Y., Yang, M., Tian, C., Jiang, S., Wang, Y., Guo, H., Wang, K., and Shu, Y. (2012). Enhancement of asynchronous release from fast-spiking interneuron in human and rat epileptic neocortex. PLoS Biol. *10*, e1001324.

Jiang, M., Yang, M., Yin, L., Zhang, X., and Shu, Y. (2015). Developmental reduction of asynchronous GABA release from neocortical fast-spiking neurons. Cereb. Cortex *25*, 258–270.

Jonas, P., Bischofberger, J., Fricker, D., and Miles, R. (2004). Interneuron Diversity series: Fast in, fast out–temporal and spatial signal processing in hippocampal interneurons. Trends Neurosci. *27*, 30–40.

Kaeser, P.S., and Regehr, W.G. (2014). Molecular mechanisms for synchronous, asynchronous, and spontaneous neurotransmitter release. Annu. Rev. Physiol. *76*, 333–363.

Kapfer, C., Glickfeld, L.L., Atallah, B.V., and Scanziani, M. (2007). Supralinear increase of recurrent inhibition during sparse activity in the somatosensory cortex. Nat. Neurosci. *10*, 743–753.

Kawaguchi, Y. (2001). Distinct firing patterns of neuronal subtypes in cortical synchronized activities. J. Neurosci. *21*, 7261–7272.

Kawaguchi, Y. (2017). Pyramidal Cell Subtypes and Their Synaptic Connections in Layer 5 of Rat Frontal Cortex. Cereb. Cortex *27*, 5755–5771.

Kawamura, Y., Nakayama, H., Hashimoto, K., Sakimura, K., Kitamura, K., and Kano, M. (2013). Spike timing-dependent selective strengthening of single climbing fibre inputs to Purkinje cells during cerebellar development. Nat. Commun. *4*, 2732.

Koester, H.J., and Johnston, D. (2005). Target cell-dependent normalization of transmitter release at neocortical synapses. Science *308*, 863–866.

Lu, T., and Trussell, L.O. (2000). Inhibitory transmission mediated by asynchronous transmitter release. Neuron *26*, 683–694.

Luo, F., and Südhof, T.C. (2017). Synaptotagmin-7-Mediated Asynchronous Release Boosts High-Fidelity Synchronous Transmission at a Central Synapse. Neuron *94*, 826–839.e3.

Manseau, F., Marinelli, S., Méndez, P., Schwaller, B., Prince, D.A., Huguenard, J.R., and Bacci, A. (2010). Desynchronization of neocortical networks by asynchronous release of GABA at autaptic and synaptic contacts from fast-spiking interneurons. PLoS Biol. *8*, e1000492.

Markram, H., Toledo-Rodriguez, M., Wang, Y., Gupta, A., Silberberg, G., and Wu, C. (2004). Interneurons of the neocortical inhibitory system. Nat. Rev. Neurosci. *5*, 793–807.

Maximov, A., Lao, Y., Li, H., Chen, X., Rizo, J., Sørensen, J.B., and Südhof, T.C. (2008). Genetic analysis of synaptotagmin-7 function in synaptic vesicle exocytosis. Proc. Natl. Acad. Sci. USA *105*, 3986–3991.

Miki, T., Nakamura, Y., Malagon, G., Neher, E., and Marty, A. (2018). Two-component latency distributions indicate two-step vesicular release at simple glutamatergic synapses. Nat. Commun. *9*, 3943.

Mittmann, W., Chadderton, P., and Häusser, M. (2004). Neuronal microcircuits: frequency-dependent flow of inhibition. Curr. Biol. *14*, R837–R839.

Moore, C.I., Carlen, M., Knoblich, U., and Cardin, J.A. (2010). Neocortical interneurons: from diversity, strength. Cell *142*, 189–193.

Muñoz, W., Tremblay, R., Levenstein, D., and Rudy, B. (2017). Layer-specific modulation of neocortical dendritic inhibition during active wakefulness. Science *355*, 954–959.

Murayama, M., Pérez-Garci, E., Nevian, T., Bock, T., Senn, W., and Larkum, M.E. (2009). Dendritic encoding of sensory stimuli controlled by deep cortical interneurons. Nature *457*, 1137–1141.

Neske, G.T., and Connors, B.W. (2016). Distinct Roles of SOM and VIP Interneurons during Cortical Up States. Front. Neural Circuits *10*, 52.

Nigro, M.J., Hashikawa-Yamasaki, Y., and Rudy, B. (2018). Diversity and Connectivity of Layer 5 Somatostatin-Expressing Interneurons in the Mouse Barrel Cortex. J. Neurosci. *38*, 1622–1633.

Oberlaender, M., Boudewijns, Z.S., Kleele, T., Mansvelder, H.D., Sakmann, B., and de Kock, C.P. (2011). Three-dimensional axon morphologies of individual layer 5 neurons indicate cell type-specific intracortical pathways for whisker motion and touch. Proc. Natl. Acad. Sci. USA *108*, 4188–4193.

Otsuka, T., and Kawaguchi, Y. (2009). Cortical inhibitory cell types differentially form intralaminar and interlaminar subnetworks with excitatory neurons. J. Neurosci. *29*, 10533–10540.

Pala, A., and Petersen, C.C.H. (2015). In vivo measurement of cell-type-specific synaptic connectivity and synaptic transmission in layer 2/3 mouse barrel cortex. Neuron *85*, 68–75.

Pouille, F., and Scanziani, M. (2004). Routing of spike series by dynamic circuits in the hippocampus. Nature *429*, 717–723.

Rahamimoff, R., and Yaari, Y. (1973). Delayed release of transmitter at the frog neuromuscular junction. J. Physiol. *228*, 241–257.

Rozov, A., Burnashev, N., Sakmann, B., and Neher, E. (2001). Transmitter release modulation by intracellular Ca2+ buffers in facilitating and depressing nerve terminals of pyramidal cells in layer 2/3 of the rat neocortex indicates a target cell-specific difference in presynaptic calcium dynamics. J. Physiol. *531*, 807–826.

Ruiz, R., Casañas, J.J., Torres-Benito, L., Cano, R., and Tabares, L. (2010). Altered intracellular Ca2+ homeostasis in nerve terminals of severe spinal muscular atrophy mice. J. Neurosci. *30*, 849–857.

Sanchez-Vives, M.V., and McCormick, D.A. (2000). Cellular and network mechanisms of rhythmic recurrent activity in neocortex. Nat. Neurosci. *3*, 1027–1034.

Silberberg, G. (2008). Polysynaptic subcircuits in the neocortex: spatial and temporal diversity. Curr. Opin. Neurobiol. *18*, 332–337.

Silberberg, G., and Markram, H. (2007). Disynaptic inhibition between neocortical pyramidal cells mediated by Martinotti cells. Neuron *53*, 735–746.

Stefanelli, T., Bertollini, C., Lüscher, C., Muller, D., and Mendez, P. (2016). Hippocampal Somatostatin Interneurons Control the Size of Neuronal Memory Ensembles. Neuron *89*, 1074–1085.

Steriade, M., Timofeev, I., Dürmüller, N., and Grenier, F. (1998). Dynamic properties of corticothalamic neurons and local cortical interneurons generating fast rhythmic (30-40 Hz) spike bursts. J. Neurophysiol. *79*, 483–490.

Steriade, M., Timofeev, I., and Grenier, F. (2001). Natural waking and sleep states: a view from inside neocortical neurons. J. Neurophysiol. *85*, 1969–1985.

Turecek, J., and Regehr, W.G. (2018). Synaptotagmin 7 Mediates Both Facilitation and Asynchronous Release at Granule Cell Synapses. J. Neurosci. *38*, 3240–3251.

Turecek, J., and Regehr, W.G. (2019). Neuronal Regulation of Fast Synaptotagmin Isoforms Controls the Relative Contributions of Synchronous and Asynchronous Release. Neuron *101*, 938–949.e4.

Turecek, J., Jackman, S.L., and Regehr, W.G. (2017). Synaptotagmin 7 confers frequency invariance onto specialized depressing synapses. Nature *551*, 503–506.

Urban-Ciecko, J., and Barth, A.L. (2016). Somatostatin-expressing neurons in cortical networks. Nat. Rev. Neurosci. *17*, 401–409.

Urban-Ciecko, J., Jouhanneau, J.S., Myal, S.E., Poulet, J.F.A., and Barth, A.L. (2018). Precisely Timed Nicotinic Activation Drives SST Inhibition in Neocortical Circuits. Neuron *97*, 611–625.e5.

Volynski, K.E., and Krishnakumar, S.S. (2018). Synergistic control of neurotransmitter release by different members of the synaptotagmin family. Curr. Opin. Neurobiol. *51*, 154–162.

Wadel, K., Neher, E., and Sakaba, T. (2007). The coupling between synaptic vesicles and Ca2+ channels determines fast neurotransmitter release. Neuron *53*, 563–575.

Wang, Y., Toledo-Rodriguez, M., Gupta, A., Wu, C., Silberberg, G., Luo, J., and Markram, H. (2004). Anatomical, physiological and molecular properties of Martinotti cells in the somatosensory cortex of the juvenile rat. J. Physiol. *561*, 65–90.

Wen, H., Linhoff, M.W., McGinley, M.J., Li, G.L., Corson, G.M., Mandel, G., and Brehm, P. (2010). Distinct roles for two synaptotagmin isoforms in synchronous and asynchronous transmitter release at zebrafish neuromuscular junction. Proc. Natl. Acad. Sci. USA *107*, 13906–13911.

Williams, S.R., and Stuart, G.J. (1999). Mechanisms and consequences of action potential burst firing in rat neocortical pyramidal neurons. J. Physiol. *521*, 467–482.

Wilson, N.R., Runyan, C.A., Wang, F.L., and Sur, M. (2012). Division and subtraction by distinct cortical inhibitory networks in vivo. Nature *488*, 343–348.

Yang, L., Wang, B., Long, C., Wu, G., and Zheng, H. (2007). Increased asynchronous release and aberrant calcium channel activation in amyloid precursor protein deficient neuromuscular synapses. Neuroscience *149*, 768–778.

Yao, J., Gaffaney, J.D., Kwon, S.E., and Chapman, E.R. (2011). Doc2 is a Ca2+ sensor required for asynchronous neurotransmitter release. Cell *147*, 666–677.

Yu, J., Hu, H., Agmon, A., and Svoboda, K. (2019). Recruitment of GABAergic Interneurons in the Barrel Cortex during Active Tactile Behavior. Neuron *104*, 412–427.e4.

Zhu, J., Jiang, M., Yang, M., Hou, H., and Shu, Y. (2011). Membrane potential-dependent modulation of recurrent inhibition in rat neocortex. PLoS Biol. *9*, e1001032.

Zucca, S., D'Urso, G., Pasquale, V., Vecchia, D., Pica, G., Bovetti, S., Moretti, C., Varani, S., Molano-Mazón, M., Chiappalone, M., et al. (2017). An inhibitory gate for state transition in cortex. eLife *6*, e26177.

STAR★METHODS

KEY RESOURCES TABLE

REAGENT or RESOURCE	SOURCE	IDENTIFIER
Antibodies		
Goat polyclonal anti-Somatostatin	Santa Cruz Biotechnology	Cat# sc-7819; RRID: AB_2302603
Donkey anti-Goat IgG H&L (Cy3) Secondary Antibody	Abcam	Cat# ab6949; RRID: AB_955018
Mouse monoclonal anti-Synaptotagmin-7 (clone N275/14)	UC Davis/NIH NeuroMab Facility	Cat# 75-265; RRID: AB_11030371
Guinea Pig polyclonal anti-vGlut1	Synaptic Systems	Cat# 135 304; RRID: AB_887878
Rabbit monoclonal anti-NeuN	Abcam	Cat# ab177487; RRID: AB_2532109
Goat anti-Mouse IgG Secondary Antibody, Alexa Fluor 488	Thermo Fisher Scientific	Cat# A-11001; RRID: AB_2534069
Goat anti-Rabbit IgG Secondary Antibody, Alexa Fluor 555	Thermo Fisher Scientific	Cat# A-21428; RRID: AB_2535849
Goat anti-Guinea Pig IgG Secondary Antibody, Alexa Fluor 647	Thermo Fisher Scientific	Cat# A-21450; RRID: AB_2735091
Chemicals, Peptides, and Recombinant Proteins		
Streptavidin, Alexa Fluor 488-conjugated	Thermo Fisher Scientific	Cat# S11223
Streptavidin, Alexa Fluor 647-conjugated	Thermo Fisher Scientific	Cat# S21374
Biocytin	Sigma-Aldrich	B4261; CAS: 576-19-2
CNQX	Tocris	0190; CAS: 115066-14-3
EGTA	Sigma-Aldrich	03777; CAS: 67-42-5
EGTA-AM	Thermo Fisher Scientific	Cat# E1219
Green fluorescent RetroBeads™	Lumafluor Inc.	https://lumafluor.com/
Red fluorescent RetroBeads™	Lumafluor Inc.	https://lumafluor.com/
Experimental Models: Organisms/Strains		
Mouse: SST-IRES-Cre	The Jackson Laboratory	JAX:013044; RRID: IMSR_JAX:013044
Mouse: PV-IRES-Cre	The Jackson Laboratory	JAX: 008069; RRID: IMSR_JAX:008069
Mouse: Ai9	The Jackson Laboratory	JAX:007909; RRID: IMSR_JAX:007909
Mouse: Ai35	The Jackson Laboratory	JAX:012735; RRID: IMSR_JAX:012735
Mouse: Synaptotagmin-7 KO (B6;129-Syt7^{tm1Sud}/J)	The Jackson Laboratory	JAX: 006388; RRID: IMSR_JAX:006388
Software and Algorithms		
MATLAB	MATHWORKS	https://www.mathworks.com/; RRID: SCR_001622
ImageJ	NIH	https://imagej.net/Welcome; RRID: SCR_003070
Mini Analysis Program	Synaptosoft Inc.	http://www.synaptosoft.com/; RRID: SCR_002184
Spike2 Software	Cambridge Electronic Design	http://ced.co.uk/downloads/latestsoftware; RRID: SCR_000903
Signal Software	Cambridge Electronic Design	http://ced.co.uk/downloads/latestsoftware

LEAD CONTACT AND MATERIALS AVAILABILITY

This study did not generate new unique reagents. Further information and requests for common resource may be directed to and will be fulfilled by the Lead Contact, Dr. Yousheng Shu (yousheng@fudan.edu.cn).

EXPERIMENTAL MODEL AND SUBJECT DETAILS

The Animal Advisory Committee at the State Key Laboratory of Cognitive Neuroscience and Learning, Beijing Normal University, approved the experimental protocols. The use and care of laboratory animals complied with the guidelines of this committee. Animals were group housed under standard conditions with *ad libitum* access to water and food. Sprague Dawley (SD) rats including juveniles

(15-20 days old) and adults (250-350 g in weight, 50-60 days old) were purchased from Beijing Vital River Laboratory Animal Technology Co., Ltd., PV^{Cre} (Jax: 008069) or $SST(SOM)^{Cre}$ (Jax: 013044) were crossed with $Ai9^{tdTomato}$ (Jax: 007909) to obtain offsprings expressing tdTomato in neocortical PV- or SST-expressing interneurons. We also crossed $SST(SOM)^{Cre}$ with $Ai35^{Arch-GFP}$ mice (Jax: 012735) to obtain offsprings with SST-positive cells expressing yellow light-activated proton pump archaerhodopsin-3 (Arch). Syt7 KO mice (Jax: 006388) (Maximov et al., 2008) were used to examine the role of Syt7 in the occurrence of AR. All these mice sacrificed for slice recording were 15-20 days old. Juvenile animals of either sex were randomly assigned to experimental conditions.

METHOD DETAILS

Slice preparation

Parasagittal slices of the SSC were obtained from postnatal day 15-20 SD rats and mice of either sex mentioned above. In some experiments, we also obtained coronal slices from PFC of SD rats with similar ages. Animals were anesthetized with sodium pentobarbital (50 mg/kg) and then decapitated. The brains were dissected out and immersed in an ice-cold sucrose-based ACSF (NaCl was replaced by equiosmolar sucrose). Slices with a thickness of 300 or 350 μm were cut in this solution with a vibratome (VT-1200S, Leica). After slicing, they were immediately transferred to an incubation chamber filled with a normal or a divalent cation reduced ACSF (see below) and maintained at 35.5°C for 45-60 min and then at room temperature before use. For recording, individual slices were transferred to a recording chamber perfused with normal or divalent cation reduced ACSF at 34.5-35.5°C. An infrared-differential interference contrast (IR-DIC) microscope (BX-51WI, Olympus) was used for visualization of individual cells in the slice. The normal ACSF contained (in mM) 126 NaCl, 2.5 KCl, 2 $MgSO_4$, 2 $CaCl_2$, 26 $NaHCO_3$, 1.25 NaH_2PO_4 and 25 dextrose (315 mOsm, pH 7.4), and was equilibrated continuously with 95% O_2 and 5% CO_2. ACSF with low divalent cation contained 1.2 or 1 mM $CaCl_2$ and 1 mM $MgSO_4$.

Animal Surgery

For sharp electrode intracellular recording *in vivo*, we used adult male SD rats (250-350 g). The animals were anaesthetized with urethane (1.5 g/kg, i.p.) and head-fixed on a stereotactic apparatus. The craniotomy (0.5-1.0 mm) was made over the barrel cortex. The body temperature was monitored and maintained at 37°C during experiments.

To identify PCs projecting to different brain regions, we injected retrograde beads (300-500 nl) were injected to either the ipsilateral pontine nuclei (green fluorescent RetroBeads, Lumafluor), contralateral SSC (red fluorescent RetroBeads) or contralateral dorsal striatum (red beads) of SD rats at postnatal day 11-13. Four days after beads injection, rats were sacrificed for brain slice recording.

Electrophysiological Recordings

Cortical layer-5 neurons in rats, including PC, MC and FS cells, were identified by their morphology and firing properties as described previously (Markram et al., 2004; Wang et al., 2004). We performed whole-cell recordings from these types of neurons using patch pipettes with an impedance of 4–7 MΩ when filled with the normal internal solution containing (in mM) 140 K-Gluconate, 3 KCl, 2 $MgCl_2$, 0.2 EGTA, 10 HEPES, 2 Na_2ATP (285-295 mOsm, pH 7.2-7.25). In some experiments, we added 10 mM EGTA to the internal solution. We also added 0.2% biocytin to the pipette solution for post hoc staining of the recorded cells. Voltage or current clamp recordings were achieved using a Multiclamp 700B amplifier (Molecular Devices). We used Micro1401-3 or Power1401-3A together with Spike2 (version 8) and Signal (version 5, Cambridge Electronic Design) for data acquisition. Voltage and current signals were filtered at 10 and 3 kHz, respectively, and sampled at 50 kHz. The liquid junction potential (~15 mV) was not corrected for the V_m shown in the text and figures.

For whole-cell recording from synaptically connected pairs, we injected a train of current pulses (1 ms in duration, 2-5 nA in current amplitude) to the presynaptic PC in current-clamp mode to evoke APs with varying number and frequency. AP trains were evoked every 15-30 s. The postsynaptic cells were recorded at resting V_m in current-clamp mode or held at −65 mV in voltage-clamp mode. For disynaptic IPSP recording from PC-PC pairs, the postsynaptic cell was held at −50 mV in current-clamp mode to increase the Cl^- driving force. For loose-patch stimulation in presynaptic PC, the patch pipette contained normal ACSF and had a seal resistance ranging from 0.6 to 1.3 GΩ.

In experiments with extracellular stimulation, we used an isolator (ISO-Flex, AMPI) and bipolar tungsten electrodes to deliver trains of stimuli (40-120 μA, 0.1 ms) every 15-30 s. The electrode was placed at the same layer but 150-300 μm away from the recorded cell. For cell-attached recording, we obtained GΩ-seal with the cell membrane using patch pipettes filled with normal ACSF; after recording, a second pipette with K^+-based internal solution was used to re-patch the cell in whole-cell configuration and obtain its electrophysiological properties for cell identification. In some experiments, EGTA-AM (200 μM, Invitrogen) or CNQX (10 μM, Tocris) were added to the bath solution.

In experiments injecting EPSC-like current waveforms (Figure 3C), currents with AR were obtained from a PC-MC pair, whereas those without AR were obtained from the same pair with the presynaptic PC re-patched using 10 mM EGTA-containing internal solution. An example current response was injected back to MC to examine the effect of AR on the timing of evoked APs. To obtain the EPSC-like currents without AR, we averaged current responses from 10 trials and fitted individual EPSCs with a double exponential function to remove the background noise (to prevent large noise level after scaling). We then scaled the resultant current trace to

reach the same total charge of those with AR during the train, to ensure the generation of similar number of IT-APs (Figure S8B). The two types of EPSC-like currents were injected to the recorded MC alternately every 20 s (Figure 3C).

Dynamic clamp was achieved using Power1401-3A and Signal software. We averaged individual EPSCs from PC-MC pair and fitted the averaged trace with an α-synapse function: $g(t) = G_{max}*(t/\tau)*\exp(1-(t/\tau))$. The time constant τ could be then obtained and applied to generate the artificial α-synapse conductances (reversal potential: 0 mV), which were injected to the recorded MCs 40 ms after the cessation of extracellular stimulation.

Intracellular recordings were performed using sharp electrodes (30-90 MΩ) filled with 2 M potassium acetate. During recording, capacitance compensation, DC offset, and bridge balance were adjusted frequently when electrode was advancing in the cortex. The V_m signals were acquired by an AxoClamp-2B amplifier (Axon Instruments), digitized and analyzed using Micro1401-3 and Spike2 software.

Immunohistochemistry

After recording, slices with cells filled with biocytin were fixed in 4% paraformaldehyde (PFA) and 4% sucrose for 2 h. They were then rinsed in 0.01 M phosphate-buffered saline (PBS, pH 7.4) for 3 times, and transferred to 0.5% Triton X-100 for 6 h and then incubated in a blocking solution (5% BSA in PBS) for 1 h. After that, slices were incubated with the SST antibody (goat anti-SST, Santa Cruz sc-7819, 1:100) for 2 days at 4°C, and finally in secondary antibody (donkey anti-goat IgG (Cy3), Abcam ab6949, 1:500) and Streptavidin (Alexa Fluor 488/647-conjugated, Invitrogen S11223/S21374, 1:500) for 2 h. For 3D reconstruction of labeled cells, z stack images (0.75 μm per image) were acquired with an air objective (40x) on a confocal microscope (Nikon A1 plus, Japan) and processed using ImageJ.

For immunostaining of Syt7, we used tissues from WT or Syt7 KO mice. We anaesthetized the animals with sodium pentobarbital and then transcardially perfused them with normal saline (0.9%) followed by 4% PFA and 4% sucrose. Brains were post-fixed in the same PFA-sucrose solution overnight at 4°C, then immersed in 30% sucrose. Sagittal sections of the SSC and the cerebellum (20 μm in thickness) were cut in a cryostat microtome (CM1950, Leica). The sections were rinsed in 0.01 M PBS for 3 times. After rinse, we transferred them to 0.5% Triton X-100 for 30 min and a blocking solution (5% BSA in PBS) for 1 h. Sections were then incubated with primary antibodies overnight at 4°C. The primary antibodies were mouse anti-Syt7 (targeting the C2A domain, UC Davis/NIH NeuroMab Facility, clone N275/14, RRID: AB_11030371, 1:100), guinea pig anti-vGlut1 (Synaptic Systems 135304, 1:1000) and rabbit anti-NeuN (Abcam ab177487, 1:500). After a complete wash in PBS, the sections were incubated with secondary antibodies (Alexa Fluor 488 goat anti-mouse IgG, Invitrogen A11001, 1:500; Alexa Fluor 555 goat anti-rabbit IgG, Invitrogen A21428, 1:500; Alexa Fluor 647 goat anti-guinea pig IgG, Invitrogen A21450, 1:500) for 2 h at room temperature. Z stack images (0.75 μm per image) were taken with 20x air objective or 100x oil-immersion objective on the confocal microscope. For comparison of the Syt7 immunosignals in sections from WT and Syt7 KO mice, we used the same laser intensity and image acquisition parameters, and processed identically using ImageJ.

QUANTIFICATION AND STATISTICAL ANALYSIS

We performed data analysis using Spike2, MiniAnalysis (Synaptosoft) and MATLAB (MATHWORKS). Two-second-long segment of current or voltage traces before the train stimulation was considered as the baseline. In PC-PC pairs where individual disynaptic IPSPs were visible, the onset of each IPSP was the time point when the second derivative of the V_m trace reached a trough (Kawamura et al., 2013), and the onset latency of individual IPSP was the time period from the immediate preceding stimulus to its onset. The onset of the whole barrage of IPSPs, including those where individual IPSPs were not clear, was the time point (relative to the onset of presynaptic train stimulation) of the first trough of the second derivative; the offset was defined as the time when the whole barrage of disynaptic IPSPs decayed to 20% of the peak amplitude. The last peak of disynaptic IPSP was defined as the time point of the last peak of the second derivative of V_m. The duration of the disynaptic IPSP barrage was the time period from its onset to offset. The symmetry ratio was a ratio of the time period of onset-to-peak (the peak of the IPSP barrage) to that of peak-to-offset (Berger et al., 2009). The peak amplitude and the voltage integral (from the onset to offset) of disynaptic IPSP barrage were only measured from PC-PC pairs with similar V_m. The spike latency was the time period from the immediate preceding stimulus to the AP peak. The jitter of the spike latency and the onset latency of individual disynaptic IPSP were obtained from APs and IPSPs during the train stimulation, respectively.

To obtain the electrophysiological properties of putative MCs, we injected a series of 500-ms positive (10 to 400 pA) and negative current pulses (−30 to −90 pA) to the recorded cell. The resting membrane potential (RMP) was the V_m without any current injection. The input resistance (Rin) was calculated by the Ohm' law, and the V_m change in response to the negative current pulses (−60 pA) was measured from the baseline to the steady state of hyperpolarization; the membrane time constant (Tau) was obtained by fitting the initial hyperpolarizing phase with a single exponential function; the Sag ratio was the ratio of the peak amplitude of the hyperpolarization to the steady-state V_m change during the negative pulse injection. The AP threshold was defined as the V_m when the rising phase of the first AP (AP_1) in the AP train (10-30 Hz) during positive pulse injection reached 20 V/s. The AP peak amplitude was measured from the AP threshold to the peak. The AP half-width was the duration of the AP_1 at half amplitude. The AP amplitude drop (AMP drop) was defined as the amplitude decrease from AP_1 to AP_2. The after-hyperpolarization potential (AHP) was measured from the threshold to the trough of the AP_1. With positive current pulses causing 40-60 Hz firing, the spiking adaptation was quantified

by the ratio: (ISI_{last}-ISI_{1st})/ISI_{last}, cells with a ratio greater than 0.3 were considered possessing an adapting firing pattern. Rebound spikes were examined when the cell was hyperpolarized by a current pulse of −90 pA. If no rebound spikes occurred at RMP, we also depolarized the baseline V_m to examine the occurrence of rebound spikes. We obtained the average number of rebound APs among rebound cells and the percentage of these cells in all putative MCs.

To compare the strength of SR and AR among different pairs, we used MiniAnalysis to detect individual EPSC events and then transferred their time information to MATLAB for further analysis (Figure S4A). The time window for SR event was 5 ms after every stimulus during train stimulation, and the rest is considered as the IT-AR time window. The duration of the PT-AR was the time period from the cessation of train stimulation (10 ms after the time of last stimulus) to the time of the last EPSC when AR frequency decreased to the baseline frequency of spontaneous EPSC events (Jiang et al., 2012). The EPSC event number of IT-AR, PT-AR and the duration of PT-AR were obtained by averaging all recorded trails. The PT-AR charge and basal current were obtained from the averaged current trace (Figure S4B). The basal current was the sustained current in the postsynaptic cell induced by the last 10 APs during the train stimulation. The unitary synaptic strength was measured as the average peak amplitude of EPSCs induced by the first APs of PC bursts. Unless otherwise stated, the failure rate was for the unitary EPSCs. A failure occurred if the V_m fluctuation was smaller than 1.2 x SD of the baseline noise.

We used Shapiro-Wilk test for data normality test. For comparison of two groups, we used two-sample Student's t test or paired Student's t test if they were normally distributed; otherwise Mann-Whitney *U* test for unpaired data or Wilcoxon signed-rank test for paired data. For comparison of multiple groups, we used one-way or two-way ANOVA since they were normally distributed. Unless otherwise stated, group data in the main text and the figures were presented as mean ± SD and mean ± SEM, respectively. Whisker boxplots represented the median and interquartile range; whiskers represented 1.5x interquartile range.

DATA AND CODE AVAILABILITY

The datasets supporting the current study have not been deposited in a public repository yet, however, they are available from the corresponding author on request.